Numerical analysis for dynamic characteristics of bridge considering next-generation high-speed train

Soon T. Oh[1a], Dong J. Lee[1b], Seong T. Yi[*2] and Byeong J. Jeong[1c]

[1]Civil and Environmental Engineering, Seoul National University of Science and Technology, Seoul 01811, Republic of Korea
[2]Department of Civil and Environmental Engineering, Inha Technical College, Incheon 22212, Republic of Korea

Abstract. To consider the effects of the increasing speed of next-generation high-speed trains, the existing traffic safety code for railway bridges needs to be improved. This study suggests a numerical method of evaluating the new effects of this increasing speed on railway bridges. A prestressed concrete (PSC) box bridge with a 40 m span length on the Gyeongbu track sector is selected as a representative example of high-speed railway bridges in Korea. Numerical models considering the inertial mass forces of a 38-degree-of-freedom train and the interaction forces with the bridge as well as track irregularities are presented in detail. The vertical deflections and accelerations of the deck are calculated and compared to find the new effects on the bridge arising with increasing speed under simply and continuously supported boundary conditions. The ratios between the static and dynamic responses are calculated as the dynamic amplification factors (DAFs) under different running speeds to evaluate the traffic safety. The maximum deflection and acceleration caused by the running speed are indicated, and regression equations for predicting these quantities based on the speed are also proposed.

Keywords: dynamic amplification factors; next-generation high-speed train; PSC box bridge; traffic safety; vertical deflections and accelerations

1. Introduction

In response to dramatic expansion in the high-speed train market, major countries, including Korea, are competing in technical development to increase the running speed of trains. The highest speed record to date is 603 km/h, set by the SCMaglev in Japan in 2015; on the other hand, the record without a maglev system is 575 km/h, set by the TGV in France in 2007. Recently, the Al Boraq high-speed rail service in Morocco has been operating on a 186-km sector with a speed of 320 km/h since November 2018. It is the first high-speed rail service in Africa. The Haramain high-speed railway in Saudi Arabia also opened to serve a 448-km sector at a 300 km/h speed in September 2019. In Korea, a 574-km sector of high-speed rail operating at 305 km/h has been in

*Corresponding author, Professor, E-mail: yist@inhatc.ac.kr
[a] Professor, E-mail: alicia@seoultech.ac.kr
[b] Ph.D. Lector, E-mail: djlee@seoultech.ac.kr
[c] M.D. Researcher, E-mail: 20510217@seoultech.ac.kr

service since 2004, and the Highspeed Electric Multiple Unit-430km/h eXperiment (HEMU-430X) succeeded in achieving a maximum speed of 421.4 km/h in 2013.

The SCMaglev technology developed by JR Central in Japan is an electrodynamic system (EDS). This system uses a completely different type of track than conventional rolling stock. Instead of metal rails, an EDS uses superconductive magnets in the train's body, which interact with metal coils along a guideway. This interaction propels the train forward and stabilizes it, and once the train is at speed, it achieves levitation at a height of 10 cm. This levitation eliminates friction, allowing these trains to reach record-breaking speeds. The lack of friction on an EDS maglev line also means that the system requires less maintenance due to mechanical wear and tear and provides a more comfortable and quieter ride for passengers. Apart from the unique features of maglev rolling stock, the reliability and convenience of this train system have made it an indispensable part of travel throughout its service area. This distinctive train system has been achieved through a variety of technologies, including aerodynamic body design, a sophisticated track system, and a computerized automated train control (ATC) network (Tsunagu Japan 2020). The SCMaglev has many great advantages, as discussed above, but requires new construction of dedicated tracks.

The Gyeongbu sector in Korea, whose construction was completed in 2010, has a bridge length of 114.5 km, 28.7% of the total track length of 418.7 km. The Honam sector, completed 5 years later, has a dramatically increased bridge proportion of 48.4%, corresponding to 111.7 of the 231.0 km of total track length. Prestressed concrete (PSC) box bridges are the major bridge type in both train sectors for a variety of reasons, including minimizing dynamics, improving traffic safety, limiting discomfort due to vibration and noise, and saving maintenance costs due to corrosion and fatigue. The PSC box bridge sections were improved to be more economical and stable during the design stage of the Honam sector. A new-generation train, including the HEMU-430X improvements and running at a higher speed of over 300 km/h, will be operated on the existing PSC box bridges in both train sectors (Cho *et al*. 2010, 2012, and Lee *et al*. 2013). Therefore, it is important to evaluate the responses of the existing bridges to the effects of the speed increase that will be imposed on them.

For the numerical analysis of the dynamic characteristics of PSC box bridges, two configurations are modeled: a simply supported bridge with a span length of 40 m and a two-span continuous bridge of the same span length in the Gyeongbu sector. A train-bridge interaction analysis is carried out with the 4th-order Runge–Kutta method to consider the inertial mass forces of a Korean Train Express (KTX) train with 38 degrees of freedom (DOFs) as well as bridge track irregularities. The magnitudes of the interaction forces at the end of each time interval are determined to solve the equations of motion for the train–bridge system. The calculated forces in the train-bridge system between the axles and the irregularly surfaced track and bridge are generated using a formula for the stiffness and deformation of the suspension assembly with springs connecting the train car body, two bogies and four axles. The displacement, velocity and acceleration of the bridge for a given running speed are calculated at the location where the maximum responses occur, usually at the midspan of the bridge. The running speeds considered in this study range from 100 to 600 km/h in 10 km/h increments at a constant speed on the bridge.

2. Train-track-bridge dynamic interaction model

The dynamic characteristics of bridges under moving trains are important in the design of PSC box bridges for high-speed railways. A train moving force model adopted from international code

UIC LM-71, corresponding to train load HL-25 of the Korean standard, is used in the actual bridge design. To describe the dynamic characteristics of the train–bridge interaction (TBI) system, a 38-DOF train model has been used as the basis for a TBI model with a two-layer (body and bogie) suspension and an irregular track surface. This TBI model consists of the constant load of the train, with m_c, m_b and m_w denoting the masses of the car body, bogie and wheel, respectively; k_p, c_p, k_s and c_s, representing the individual spring stiffnesses and damping effects of the primary and secondary suspension systems; and k and c, representing the combined stiffness and damping of the primary and secondary suspension systems. The discrete equation of train motion is written as follows:

$$M_T \ddot{u}_T + C_T \dot{u}_T + k_T u_T = f_T \tag{1}$$

where the subscript T refers to the train system; M, C and k are the mass (m_c, m_b and m_w), damping (c_p and c_s), and stiffness (k_p and k_s) matrices, respectively; and u is the displacement vector. The train force vector, f_T, contains the dynamic interaction forces.

The track–bridge system is coupled with the train system to iteratively solve for the dynamic interaction forces. The equation of track–bridge motion is written as follows:

$$M_{TB} \ddot{u}_{TB} + C_{TB} \dot{u}_{TB} + k_{TB} u_{TB} = f_{TB} \tag{2}$$

where the subscript TB refers to the track–bridge system. The track–bridge force vector, f_{TB}, is composed of the static load from the train as well as dynamic interaction forces.

2.1 Numerical simulation procedure

The TBI model is not the moving constant model adopted in most national design codes as a conservative load, but it is a fundamental concern in the field of railway engineering. Here, the numerical simulation procedure using the TBI model is systematically explained, including the train model, the bridge model, the modeling of the track irregularity and the TBI, the system excitation and the solution algorithm. The train–bridge model adopts the rigid wheel–rail coupling contact assumption; the wheel displacement, u_W, is restricted to follow the point of contact with the track plus the track irregularity r_W. Thus, the DOF of the wheel is eliminated. The DOFs of the train are also reduced to those of a suspended body. The constraint equations for displacement, velocity and acceleration are given below:

$$u_w = \mathbf{N}\mathbf{u}_{T,i} + r_w \tag{3a}$$

$$\dot{u}_w = \mathbf{N}\dot{\mathbf{u}}_{T,i} + v\mathbf{N}'\mathbf{u}_{T,i} + vr'_w \tag{3b}$$

$$\ddot{u}_w = \mathbf{N}\ddot{\mathbf{u}}_{T,i} + 2v\mathbf{N}\dot{\mathbf{u}}_{T,i} + a\mathbf{N}'\mathbf{u}_{T,i} + v^2\mathbf{N}''\mathbf{u}_{T,i} + ar'_w + v^2 r''_w \tag{3c}$$

where N is the cubic shape function of the beam element evaluated at the point of contact with the i-th wheel set, $u_{T,i}$ is the vertical displacement vector of the beam element in contact, the prime operator means the differential of the vertical displacement and v and a are the running speed and acceleration of the train.

Based on the rigid contact assumption, the TBI system can be described by a coupled equation of motion with time-dependent matrices:

$$\begin{bmatrix} M_V & 0 & 0 \\ 0 & M_T + M_V & 0 \\ 0 & 0 & M_B \end{bmatrix} \begin{bmatrix} \ddot{\mathbf{u}}_V \\ \ddot{\mathbf{u}}_T \\ \ddot{\mathbf{u}}_B \end{bmatrix} + \begin{bmatrix} C_V & C_{V,T} & 0 \\ C_{T,V} & C_T + C_W & C_{T,B} \\ 0 & C_{B,T} & C_B \end{bmatrix} \begin{bmatrix} \dot{\mathbf{u}}_V \\ \dot{\mathbf{u}}_T \\ \dot{\mathbf{u}}_B \end{bmatrix} + \begin{bmatrix} K_V & K_{V,T} & 0 \\ K_{T,V} & K_T + K_W & K_{T,B} \\ 0 & K_{B,T} & K_B \end{bmatrix} \begin{bmatrix} u_V \\ u_T \\ u_B \end{bmatrix} = \begin{bmatrix} f_V \\ f_T \\ f_B \end{bmatrix} \tag{4}$$

where subscripts V, T and B refer to the vehicle, track and bridge subsystems, respectively, and W refers to the coupling terms from each vehicle wheel. The vehicle–track coupling depends on the location of the vehicle and should be updated in each time step (Therese 2018).

2.2 Bridge system

Two types of bridge systems are selected, namely, a simply supported bridge and a two-span continuous bridge, based on existing bridges along the Gyeongbu high-speed train line. The span length of 40 m is the longest among the PSC box bridges on this train line and thus is considered as the critical structural situation. In the case of the simply supported PSC box bridge, a three-dimensional beam element model including 440 nodes, 600 elements, and 43 material properties is generated, with 40 nodes per section of 4 m each and 440 transverse elements connecting 160 longitudinal elements. The bridge mass is modeled as a consistent mass instead of a lumped mass to consider the resonance effect in detail as well as a 5% damping ratio. A PSC box with a width if 14 m and a height of 2.5 m is modeled. In the case of the two-span continuous bridge, the same PSC box section is adopted to enable comparison with the dynamic responses of the simply supported bridge under identical conditions. The analyzed interval of running time is 0.0004 sec. The outputs of the solution procedure are divided into two types: 6-direction displacements, velocities and accelerations for nodes and 6-direction reactions for elements (Moazam *et al*. 2017 and Oh *et al*. 2021).

2.3 Vehicle system

The KTX power vehicle consists of one body, two bogies and four wheel-sets independently connected by springs and dampers, forming the primary and secondary suspension systems. The equations of motion of the train characterized by the bogie system are derived from Lagrangian equations considering the car body, two bogies and four wheel-sets in three dimensions. Each independent mass of the car body and the bogies has 6 DOFs corresponding to three translations, including longitudinal motion, sway and bounce, as well as the rotations, the so-called pitch, roll and yaw. For the four wheel-sets, only 5-DOF motion is allowed, without any pitching motion. Therefore, the KTX vehicle system is modeled with a total of 38 DOFs. The equation of motion is represented in Eq. (1) (Oh *et al*. 2010).

2.4 Track irregularity

Track irregularity is a factor concerned with minor imperfections in materials and tolerance errors arising in manufacturing or construction. To numerically define the track irregularity, we define four geometrical indices: the alignment and gauge for layout and the cross-level and vertical profiles for elevation.

$$S(\emptyset)_{a,v} = \frac{A\emptyset_2^2(\emptyset^2 + \emptyset_1^2)}{\emptyset^4(\emptyset^2 + \emptyset_2^2)} \tag{5a}$$

$$S(\emptyset)_{c,g} = \frac{A\emptyset_2^2}{(\emptyset^2 + \emptyset_1^2)(\emptyset^2 + \emptyset_2^2)} \tag{5b}$$

where subscripts *a, g, c*, and *v* refer to the alignment, gauge, cross-level profile and vertical profile,

respectively. $S(\emptyset)$ is the power spectral density (PSD) function. A is the roughness parameter $(m^2 \cdot (rad/m))$, and $\emptyset$ is the break frequency (rad/m) (Kim 2000 and Suh 2015).

Using the PSD function, 9 classes of track irregularity have been generated by the Federal Railroad Administration (FRA). Although track class 9 is suggested for high speeds of up to 350 km/h, this maximum speed is not sufficient for our purposes; therefore, it is necessary to generate three further classes using an identical procedure.

3. Dynamic characteristics of PSC box railway bridges

According to the Korean Traffic Safety Code, a bridge with a 40 m span length must satisfy three limiting criteria: the maximum deck deflection must be under 23.5 mm, the deflection acceleration must be below 0.35g (3.50 m/sec^2), and the vertical profile of the deck must be within 1.2 mm over 3 m. Moreover, the acceleration felt by passengers on the train must be under 0.20g (2.00 m/sec^2) according to the riding comfort code. The maximum vertical deflections of the bridges as a function of train speed are shown in Fig. 1.

The static responses in the two bridge cases are 3.82 mm for the simply supported bridge and 2.96 mm for the continuously supported bridge. In the case of the simply supported bridge, the critical results are expected, and the peak total vertical deflection within the analyzed speed range is calculated to be 11.82 mm at a speed of 390 km/h. Within the KTX maximum speed of 300 km/h, the peak is 9.52 mm at a speed of 290 km/h. In the case of the continuously supported bridge, the peak responses are 8.82 mm at a speed of 420 km/h at the first midspan and 10.16 mm at a speed of 570 km/h at the second midspan.
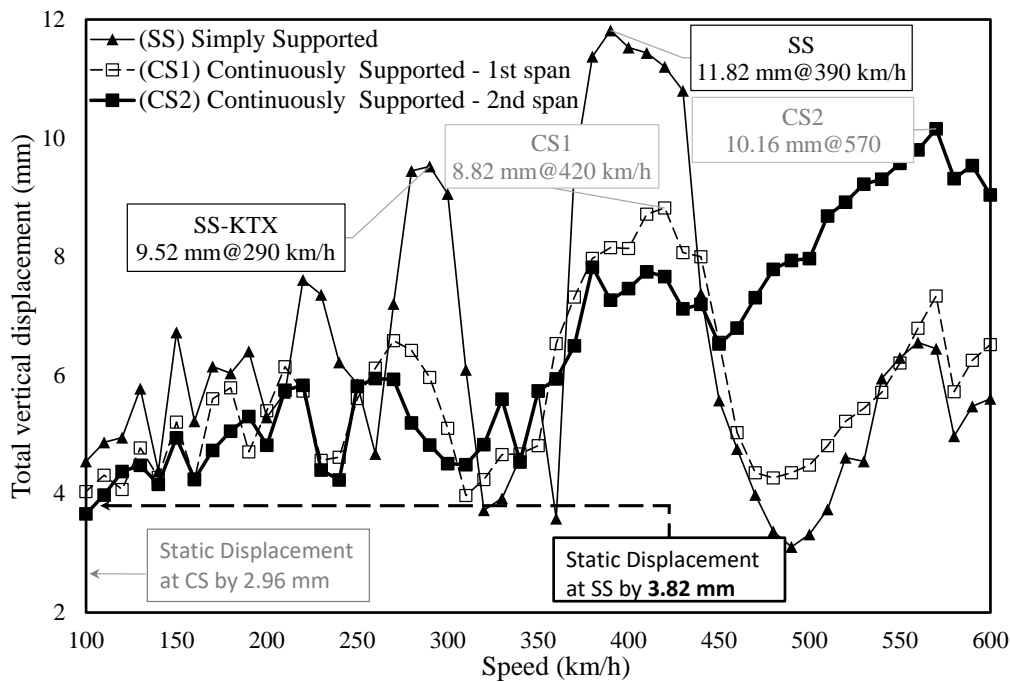

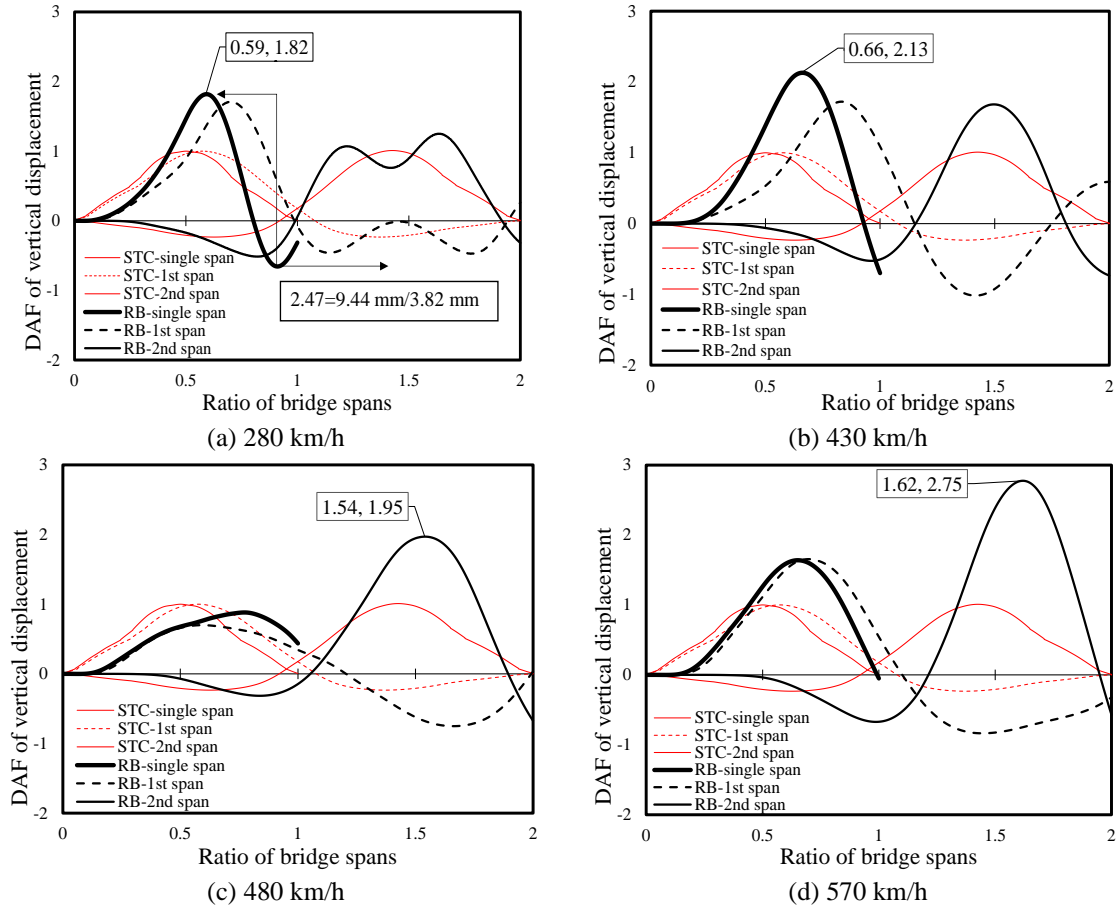Fig. 1 Total vertical displacement vs. train speed

(a) 280 km/h

(b) 430 km/h

(c) 480 km/h

(d) 570 km/h

Fig. 2 DAFs at typical speeds

3.1 Dynamic amplification factor (DAF)

The DAF is defined as the ratio of the dynamic response over the static response due to an external moving train load. Unfortunately, there is a certain amount of ambiguity regarding how to calculate the tolerance to an increase in speed. The DAFT, considering the total behavior between the maximum and minimum responses, is needed to define the actual behavior of a bridge as a critical condition value. The DAFs of 3 measuring points at typical speeds are shown in Fig. 2. These points are expected to be the points of maximum deflection of the bridges; they are located at the midspans and on the right-bottom (RB) side of the corresponding section, assuming that the train is on the right side.

The maximum DAF at 280 km/h in Fig. 2(a) indicates a dynamic deflection of 1.82 times the static deflection of 3.82 mm for the single-span bridge, which occurs at 0.59 of the span length. The DAFT is 2.47, corresponding to a total deflection of 9.44 mm (a positive deflection of 6.94 mm plus a negative deflection of 2.50 mm). Within this speed range, the DAF and DAFT of the single-span bridge are higher than those of the others. This is also true throughout the speed range depicted in Fig. 1.
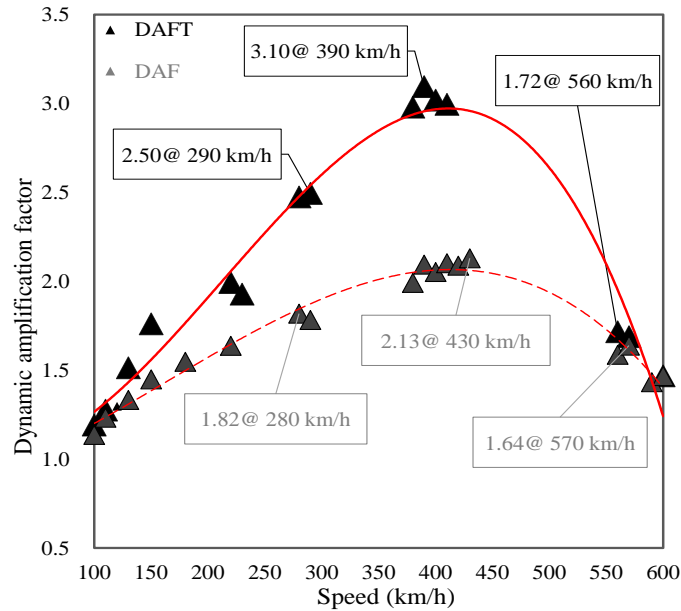
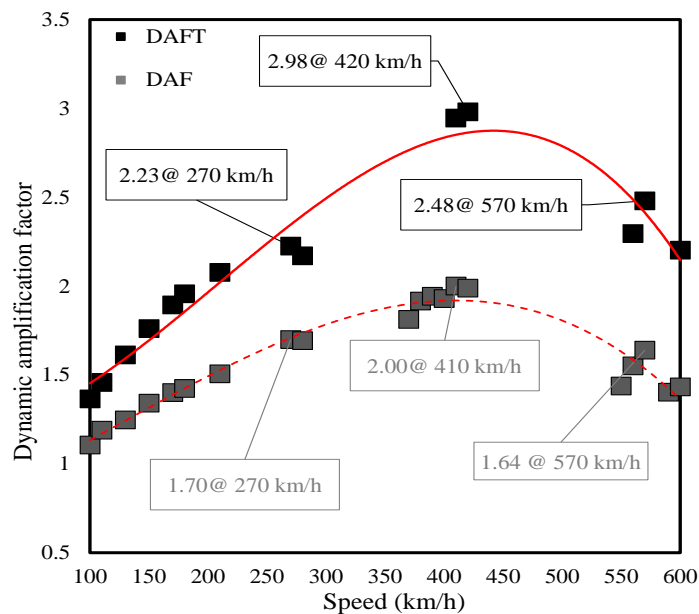Fig. 3 DAFT of the simply supported bridge

Fig. 4 DAFT of the 1st span of the continuously supported bridge

The maximum DAF at the speed of 430 km/h shown in Fig. 2(b) indicates a dynamic deflection of 2.13 times the static deflection of 3.82 mm for the single-span bridge, which occurs at 0.66 of the total span length. The DAFT is 2.83 (corresponding to a total deflection of 10.80 mm = 8.13 mm+2.67 mm). The DAFTs of the other points at the 1st and 2nd span are increased to 2.43 and 2.09, respectively, at a speed of 420 km/h. This means that the DAF of the single-span bridge is

still higher, but the maximum deflection is slightly delayed from the midspan of the bridge. On the other hand, the maximum DAF at the speed of 480 km/h shown in Fig. 2(c) indicates a dynamic deflection of 1.95 times the static deflection of 2.96 mm for the continuously supported bridge, which occurs in the second span at 1.54 of the total length of two spans. The DAFT is 2.13 (corresponding to a total deflection of 7.78 mm = 5.80 mm+1.98 mm). The DAFs of the single-span bridge and the first span of the continuously supported bridge decrease to 88% and 70% of the static response, respectively. As seen from the above analysis, the DAF and DAFT of the 2nd span of the continuously supported bridge become higher for speeds over 300 km/h.

The DAF of the 2nd span of the continuously supported bridge increases to a maximum at a speed of 570 km/h, as shown in Fig. 2(d). This peak corresponds to 2.75 times the static deflection of 2.96 mm for the 2nd span of the continuously supported bridge.

The peak point of the deflection is also delayed from the midspan, causing the dynamic response to be extended. The DAFT becomes 3.43 (corresponding to a total deflection of 8.18 mm+1.98 mm = 10.16 mm). Although the DAFs of the single-span bridge and the first span of the continuously supported bridge increase slightly to 164% and 165% of the static response, respectively, the DAF and DAFT of the 2nd span of the continuously supported bridge reach maximum values of 2.76 and 3.43, respectively, greater than those of the single-span bridge, despite the actual deflection being 11.82 mm at a speed of 390 km/h.

3.2 DAFT and DAF of the single-span bridge

The DAFT is the total sum of the positive and negative responses due to a dynamic load with a certain movement speed, expressed as a fraction of the response evaluated in a static analysis with an equivalent load. On the other hand, the DAF is usually a ratio of positive results and thus is smaller than the corresponding DAFT. The difference between DAFT and DAF increases when the negative response grows at a particular running speed. This results in a certain amount of ambiguity in how the tolerable speed increment is determined.

The DAFT and DAF results for the single-span 40 m PSC box bridge under simply supported conditions (SS) are illustrated in Fig. 3 for the same speed range. The 3rd-order polynomial trendlines generated via regression analysis using only selected results are presented below as Eqs. (6a) and (6b):

$$DAFT_{ss}=-6.20 \times 10^{-8}x^3+3.96 \times 10^{-5}x^2-1.09 \times 10^{-3}x+1.04 \tag{6a}$$

$$DAF_{ss}=-2.04 \times 10^{-8}x^3+1.01 \times 10^{-5}x^2+2.13 \times 10^{-3}x+0.91 \tag{6b}$$

where x is the running speed (km/h).

In on-site loading tests of the reference railway bridge, typical maximum deflections ranging from 1.00 mm up to 1.50 mm have been recorded, and the measured deflection induced by a full-speed running train does not exceed 1.87 mm. By comparison, the static deflection caused by a stopped train at the midspan of the bridge is usually reported to be approximately 1.48 mm (Ministry of Land, Infrastructure and Transport 2022). Based on these values, a ratio of almost 2.5 between the observed static value and the corresponding numerical static value is calculated. This bridge is a new structure, constructed within the last 10 years, so its structural properties are still of excellent quality; moreover, the reported values were measured between 2008 and 2010, although they were not published until 2020. This seems to be why the on-site test results for the measured deflections between a running train and a stopped train are reported to differ by less than 5.0%.
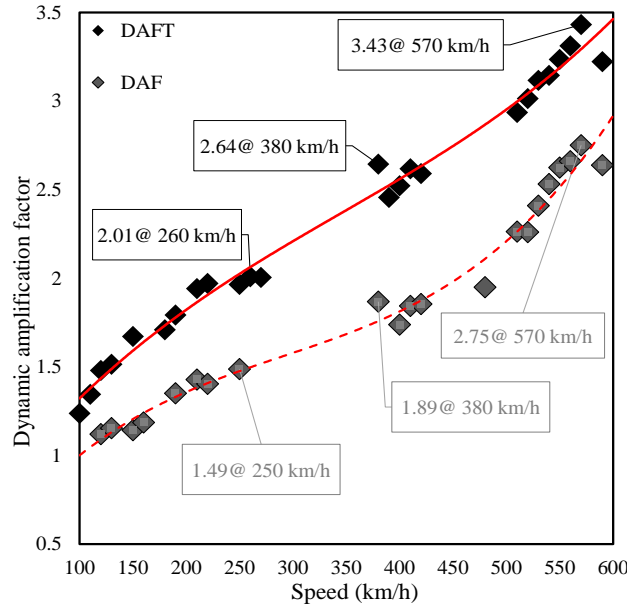
Fig. 5 DAFT of the 2nd span of the continuously supported bridge

3.3 DAFT and DAF of the 1st span of the continuously supported bridge

The DAFT and DAF of the 1st midspan of the continuously supported 40 m PSC box bridge (CS1) are illustrated in Fig. 4 for the same speed range. The 3rd-order polynomial trendlines generated via regression analysis using only selected results are presented below as Eqs. (7a) and (7b):

$$DAFT_{cs1} = -3.38 \times 10^{-8}x^3 + 2.11 \times 10^{-5}x^2 + 1.17 \times 10^{-3}x + 1.16 \tag{7a}$$

$$DAF_{cs1} = -1.46 \times 10^{-8}x^3 + 5.28 \times 10^{-6}x^2 + 3.05 \times 10^{-3}x + 0.79 \tag{7b}$$

The trend lines for $DAFT_{cs1}$ and DAF_{cs1} both have similar shapes to those for $DAFT_{ss}$ and DAF_{ss}, but the ratio of the peak values is slightly smaller than the average ratio of 73.5% over all maximum deflections. Between the DAFT values of both CS1 and SS, the ratio is close to 94%. To ensure proper comparisons with both conditions, it is better to use the predicted trend line of deflection vs. train speed than to use the DAFT value to evaluate the mechanically expected result.

3.4 DAFT and DAF of the 2nd span of the continuously supported bridge

The DAFT and DAF of the 2nd midspan of the continuously supported 40 m PSC box bridge (CS2) are illustrated in Fig. 5 for the same speed range. The 3rd-order polynomial trendlines generated via regression analysis using only selected results are presented below as Eqs. (8a) and (8b):

$$DAFT_{cs2} = 1.29 \times 10^{-8}x^3 - 1.34 \times 10^{-5}x^2 + 8.12 \times 10^{-3}x + 0.63 \tag{8a}$$

$$DAF_{cs2} = 2.02 \times 10^{-8}x^3 - 1.70 \times 10^{-5}x^2 + 7.01 \times 10^{-3}x + 0.47 \tag{8b}$$
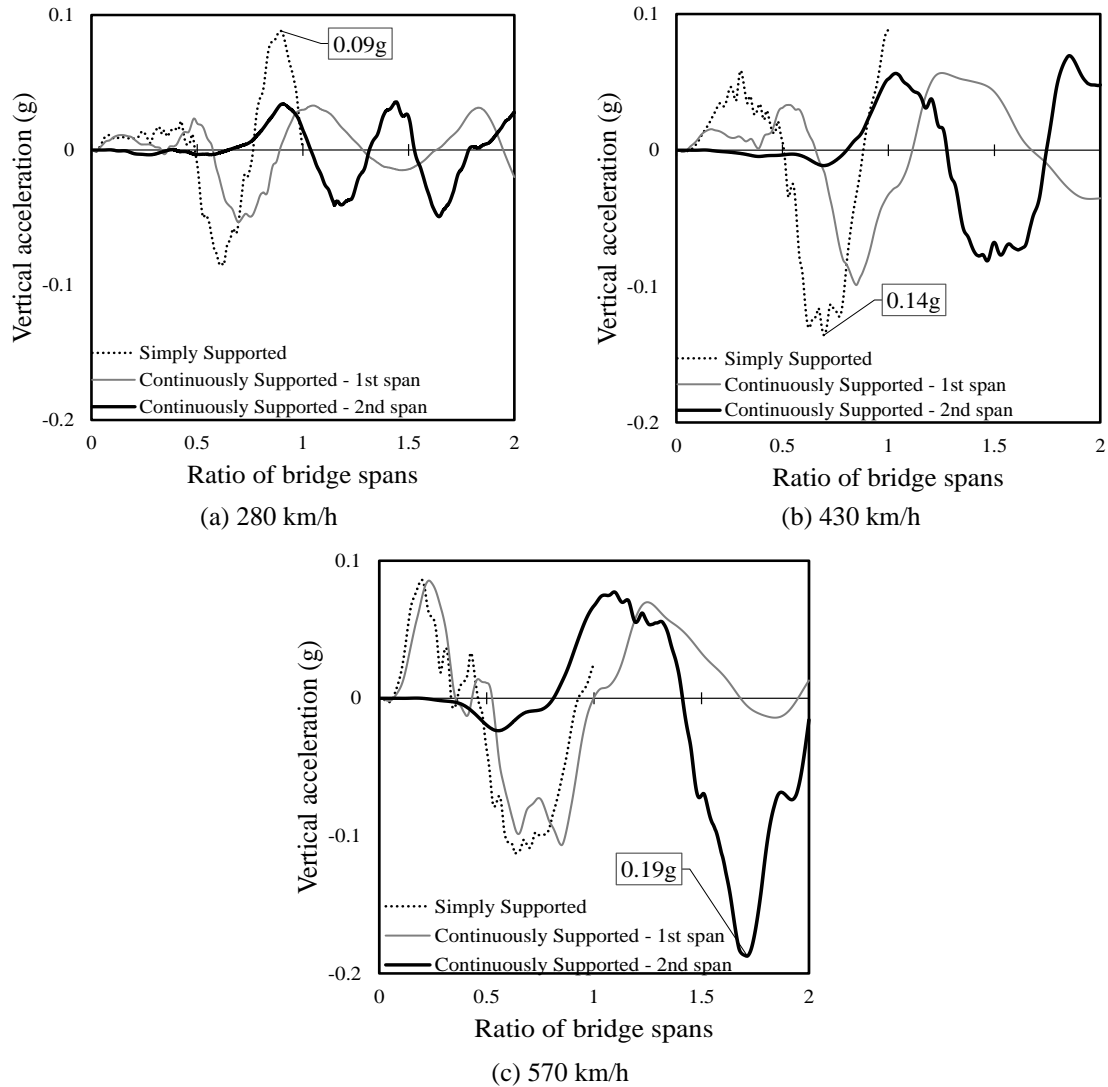
(a) 280 km/h

(b) 430 km/h

(c) 570 km/h

Fig. 6 Vertical accelerations at typical speeds

where x is the running speed (km/h).

This analysis yields the major finding that $DAFT_{cs2}$ and DAF_{cs2} continue to dramatically increase up to a speed of 600 km/h. The maximum calculated values of 3.43 for $DAFT_{cs2}$ and 2.75 for DAF_{cs2} correspond to a speed of 570 km/h. These values are the highest among all of the analyzed results; on the other hand, the actual deflection value of 10.16 mm does not exceed the maximum deflection of 11.82 mm of the single-span bridge at a speed of 390 km/h. This finding should be validated by a literature survey, but this is not possible because most research results and measured records do not include values for the speed range over 350 km/h, and the dynamic responses of the second span of a continuously supported bridge have also received little research interest. This is why an extensive, in-depth theoretical and experimental study is needed.

4. Vertical acceleration of deck deflection

According to the Korean Traffic Safety Code, a bridge with a 40-m span length must have a maximum acceleration below 0.35g. The vertical accelerations of the deck at three selected typical speeds are shown in Fig. 6. Within the existing operating speed range of KTX (below 300 km/h), the peak acceleration is controlled to no more than 0.09g for the simply supported bridge, and the accelerations of both 1st and 2nd midspans of the continuously supported bridge are within 0.05g, as illustrated in Fig. 6(a). In comparison, at a running speed of 430 km/h, a maximum vertical acceleration of 0.14g is recorded for the simply supported bridge, and the results for the 1st and 2nd midspans of the continuously supported bridge increase to 0.10g and 0.07 g, respectively, as shown in Fig. 6(b). On the other hand, the maximum acceleration at a running speed of 570 km/h is 0.19g, which is observed for the 2nd span of the continuously supported bridge, and the accelerations of the single-span bridge and the 1st span of the continuously supported bridge are no greater than 0.11g.

All analyzed accelerations satisfy the traffic safety limit of 0.35g as well as the optimistic ride comfort limit of 0.2g. The maximum vertical accelerations of the bridges within the analyzed train speed range are shown in Fig. 7. In the case of the simply supported bridge, the maximum acceleration is 0.12g at a speed of 390 km/h, and within the current operating speed range, it is only 0.09g at 280 km/h. In the other case, the maximum responses of the continuously supported bridge at the 1st and 2nd midspans are 0.12g at a speed of 430 km/h and 0.20g at a speed of 580 km/h, respectively. These values occur in the HEMU high-speed range and exceed the values observed for the simply supported bridge. In particular, it is expected that the extraordinary observations at the 2nd midspan of the continuously supported bridge might require intensive study.

5. Conclusions

In this study, a numerical simulation procedure is proposed for predicting the dynamic characteristics of PSC box railway bridges. The deflection and acceleration at the midspans of simply and continuously supported bridges on the Gyeongbu high-speed railway are predicted using TBI modeling. Prediction formulas for the DAFT and DAF are proposed and investigated as follows:

• Within the whole analyzed speed range (up to 600 km/h), the maximum calculated deflection is 11.82 mm at a speed of 390 km/h, and the maximum calculated acceleration is 0.19g at a speed of 570 km/h.

• In terms of the DAFT ratio, the maximum value of 3.43 is predicted to occur at a speed of 570 km/h at the 2nd midspan of the continuously supported bridge. In accordance with the proposed formula, the dynamic characteristics of railway bridges can be successfully determined.

• According to the Korean Traffic Safety Code, the allowable deflection and acceleration of the bridge deck are 23.5 mm and 0.35g, respectively. In our study, the maximum deflection and acceleration within the analyzed speed range up to 600 km/h are found to be below 11.82 mm (50% of the value allowed by the code) and 0.20g (54%), respectively, which successfully satisfy the traffic safety code.

• The numerical analysis of the investigated railway bridges at running speeds between 100 km/h and 600 km/h reveals that all of the calculated results satisfy not only the traffic safety code but also the riding comfort code. Despite these successful results, further intensive research is

needed to clarify the extraordinary response at the 2nd midspan of the continuously supported bridge.

Acknowledgement

References

Oh, S.T., Shim, Y.W., and Lee, D.J. (2010), "Dynamic analysis of PSC box bridge for a high-speed railway vehicle using improved 38-degree of freedom model", *J. Korea Concr. Inst.*, **22**(6), 797-803. https://doi.org/10.4334/JKCI.2010.22.6.797.

Cho, J.I, Park, T.W., Yoon, J.W., Kim, J.Y., and Kim, Y.G. (2010), "Stability and safety analysis on the next generation high-speed railway vehicle", *J. Korean Soc. Railway*, **13**(3), 245-250.

Cho, J.R, Cho, K.H., Kwark, J.W., and Kim, Y.J. (2012), "Dynamic characteristics of simply supported single span bridges for KTX and HEMU using design diagram", *J. Korean Soc. Railway*, **15**(5), 498-507. https://doi.org/10.7782/JKSR.2012.15.5.498.

Moazam, A.M., Hasani, N., and Yazdani, M. (2017), "3D simulation of railway bridges for estimation fundamental frequency using geometrical and mechanical properties", *Adv. Comput. Des.*, **2**(4), 257-271. https://doi.org/10.12989/acd.2017.2.4.257.

Oh, S.T., Lee, D.J., Jeong, B.J., Park, J.Y., and Moon, D.J. (2021), "Train wheel force analysis by dynamic analysis of high-speed train bridges", *Int. J. Eng. Innov. Technol.*, **10**(11), 1-6.

Kim, S.I. (2000), "Bridge-train interaction analysis of high-speed railway bridges", Ph.D. Dissertation, Seoul National University, Seoul, Korea.

Therese, A. (2018), "Train-track-bridge interaction for the analysis of railway bridges and train running safety", Ph.D. Dissertation, KTH Royal Institute of Technology, Sweden.

Lee, C.G., Jung, S.Y., Kim, D.H., Nam, J.W., and Hwang, K.S. (2013), *The Modification of Field Load Test for Gyeongbu High-Speed Railroad Bridges*, Magazine of the Korea Institute for Structural Maintenance and Inspection, September.

Suh, S.B. (2015), *Application of Power Spectrum Density for Evaluation of Track Quality*, Railway Journal, October.

Ministry of Land, Infrastructure and Transport (2022), "Test and evaluation method of railway bridge by load carrying capacity evaluation for safety inspection of maintenance", 20CTAP-C152026-02, Bucheon University, Seoul National University of Science and Technology, GEOKoreaENG, Airport Railroad, and SAMLIM Engineering.

Tsunagu Japan (2020), All about Japan's Maglev bullet train; The levitating high speed train set to cut travel times in half, Japan. https://www.tsunagujapan.com/japans-new-maglev-shinkansen-bullet-train.

TK